

# 1

## INTRODUCTION

---



# 2

## BIOLOGY

---



# 3

## GRAPH THEORY

---

A review of graph theory lays the foundation for the mathematical considerations in this work.

In this chapter we review basic graph theory and explain how these terms are applicable in the context of biological neural networks. We begin with the definition of directed graphs:

### 3.1 DIRECTED GRAPHS

**Definition 3.1** (Directed graphs). A *directed pseudograph*  $G$  consists of two finite  $V$ , the *set of vertices* of  $G$ , and  $E$ , the *set of edges* of  $G$ , and two maps  $s, t : E \rightarrow V$ , the *source* and *target functions* of  $G$ . A *directed multigraph* is a directed pseudograph without loops, that is the map  $d = (s, t) : E \rightarrow V^2$  already maps to  $V^2 \setminus \Delta_V$ , where  $V^2 = V \times V$  denotes the cartesian product and  $\Delta_V = \{(x, x) \mid x \in V\} \subseteq V^2$  the diagonal. Similarly, a *directed loop graph* is a directed pseudograph where  $d$  is injective. Finally, a *simple directed graph* can be defined as a directed pseudograph where  $d$  is both injective and already maps to  $V^2 \setminus \Delta_V$ .

Thus, in simple directed graphs, neither parallel edges nor loops - edges between the same vertex - are allowed, whereas directed multigraphs and directed loop graphs admit one of them respectively.

Say something about what "directed graph" means here, do all definition until random graphs work for all types of directed graphs?

Given a directed graph  $G$ , we denote with  $V(G)$  the set of vertices of  $G$  and call it the **vertex set** of  $G$ . Analogously, the **edge set**  $E(G)$  of  $G$  denotes the set of edges of  $G$ . This means, for a directed graph specified as  $G = (V, E, s, t)$ , we have  $V(G) = V$  and  $E(G) = E$ .

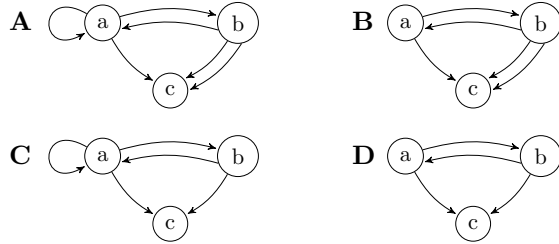


**Figure 3.1:** Typical examples of the directed graph types **A**) directed pseudograph **B**) directed multigraph **C**) directed loop graph **D**) simple directed graph.

A **morphism**  $\phi : G \rightarrow H$ , between two directed graphs  $G = (V_G, E_G, s_G, t_G)$  and  $H = (V_H, E_H, s_H, t_H)$ , consists of a pair of maps  $\phi_V : V_G \rightarrow V_H$  and  $\phi_E : E_G \rightarrow E_H$ , such that

$$s_H \circ \phi_E = \phi_V \circ s_G \quad \text{and} \quad t_H \circ \phi_E = \phi_V \circ t_G,$$

that is such that the following diagram commutes:

$$\begin{array}{ccc} E_G & \xrightarrow{\phi_E} & E_H \\ s_G \downarrow t_G & & \downarrow s_H t_H \\ V_G & \xrightarrow{\phi_V} & V_H \end{array}$$

A morphism  $\varphi : G \rightarrow H$ , between two directed pseudographs  $G$  and  $H$  is an **isomorphism**, if the maps  $\varphi_V : V_G \rightarrow V_H$  and  $\varphi_E : E_G \rightarrow E_H$  are bijective. Two directed pseudographs are called *isomorphic* if there exists an isomorphism inbetween them.

*Remark.* The last definition implies that, if there exists an isomorphism  $\varphi : G \rightarrow H$ , an isomorphism  $\psi : H \rightarrow G$  can be found. This isomorphism is, of course, easily constructed via  $\psi_V : V_H \rightarrow V_G, v \mapsto \varphi_V^{-1}(v)$ ,  $\psi_E : E_H \rightarrow E_G, e \mapsto \varphi_E^{-1}(e)$ .

**Definition 3.2** (Weighted directed graphs). An *edge-weighted directed graph* is a directed graph  $G$  along with a mapping  $\omega : E(G) \rightarrow \mathbb{R}$ , called the *weight function*. Similarly, a *vertex-weighted directed graph* is a directed graph with a mapping  $\nu : V(G) \rightarrow \mathbb{R}$ .

*Remark.* (heavy draft)

Certainly, a weighted directed pseudograph is the most fitting mathematical modelling to the biological situation, since self connections and multiple synapse are not only plausible (source?) but the rule. However there is one abstraction we can make by adding together the synaptic weights - NEST is doing it. While linear synaptic integration was shown to be, it is a prevalent model in network (ref Nest).

Also think about **inhibitory, excitatory**. Suggestion: edge weights  $\omega : E(G) \rightarrow \mathbb{R}^+$  and vertex weights  $\nu : V(G) \rightarrow \{-1, 1\}$ . Synaptic weight  $\text{syn}(e)$  for edge  $e$  is then

$$\text{syn}(e) = \nu(s(e)) \omega(e).$$

Benefit: Synapse from one neuron are either excitatory or inhibitory but not mixed as in bio.

*Remark* (Equivalent definiton for directed loop graphs). A directed loop graph  $G$  can be equivalently defined as a pair of finite(, non-empty?) sets  $V$ , the *set of vertices* of  $G$ , and  $E \subseteq V^2$  the *set of edges* of  $G$ . For an edge  $(x, y) \in E$ , we call  $x$  the *source* and  $y$  the target of the edge  $(x, y)$ .

Source and target functions are then uniquely determined as the projections on the first and second component,  $s = \text{pr}_1, t = \text{pr}_2 : E(G) \rightarrow V$ . Conversely, the edge set  $E(G) \subseteq V^2$  can be determined from the source and target functions as  $E := \{(s(e), t(e)) \mid e \in E\}$ . The trivial identities  $(x, y) = (\text{pr}_1(x, y), \text{pr}_2(x, y))$  and  $\text{pr}_1(s(e), t(e)) = s(e)$  with  $\text{pr}_2(s(e), t(e)) = t(e)$  quickly verify the equivalence of the definitions.

Given a directed loop graph  $G$ , we often assume the graph to be given in this form and write edges as  $e = (x, y)$ . Note that this concept is more complicated to introduce for directed pseudographs, since parallel edges  $e$  and  $e'$  should to be differentiated in the egde set of  $G$ , establishing the need for  $E(G)$  to be a multi- or indexed set, notions we are trying to avoid in this document.

From now on any *directed graph* is assumed to be a directed loop graph. Although most, if not all, concepts work for directed pseudographs just as well, we want to start to heavily use the canonical edge representation, which when talking about pseudographs makes problems as mentioned before.

*Remark* (More Notation). - Check, do I really need this? For a pair of vertex sets  $X, Y \subseteq V(G)$  of a directed graph  $G$  we write

$$(X, Y)_G = \{(x, y) \in E(G) \mid x \in X, y \in Y\}$$

for the set of edges with source in  $X$  and target in  $Y$ . For vertex sets with a single element  $X = x$ , we also write  $(x, Y)_G$  and mean the edges with source  $x$  and target in  $Y$ .

**Definition 3.3** (In- and out-degree). For a directed graph  $G$  the **in-degree**  $d_G^-(x)$  of a vertex  $x$  is defined as the number of edges of  $G$  with target  $x$ , that is

$$d_G^-(x) = |(V(G), x)_G|.$$

Similarly, the **out-degree**  $d_G^+(x)$  of  $x$  is defined as

$$d_G^+(x) = |(x, V(G))_G|,$$

the number of edges in  $G$  with source  $x$ .

*Remark* (Side). In some literature about directed graphs (Bang-Jensen), loops are *not* counting towards the in- or out-degree of vertex. In the light of neural network however, we specifically want to count loops as well.

A basic property of the in- and out-degree in directed graphs is that number of in-degrees of every vertex, as well the sum of every out-degree, equal the total number of edges:

**Proposition 3.4.** *In every directed graph  $G$ , we have*

$$\sum_{x \in V(G)} d^-(x) = \sum_{x \in V(G)} d^+(x) = |E(G)|.$$

*Proof.* Since  $(V(G), x)_G \cap (V(G), y)_G = \emptyset$  for  $x \neq y$ , we can write

$$\sum_{x \in V(G)} d^-(x) = \left| \bigcup_{x \in V(G)} (V(G), x)_G \right| = |(V(G), V(G))_G| = |E(G)|.$$

Analogously for the out-degree. □

### 3.2 WALKS AND DISTANCES

Let  $G$  be a directed graph ([what does it mean here?](#)). A **walk**  $W$  in  $G$  is an alternating sequence  $(x_1, e_1, x_2, e_2, x_3, \dots, x_{n-1}, e_{n-1}, x_n)$  of vertices  $x_i$  and edges  $e_i$  from  $G$ , such that

$$s(e_i) = x_i \quad \text{and} \quad t(e_i) = x_{i+1}, \quad \text{for } i = 1, \dots, n-1,$$

that is, such that the vertices are connected by the edges inbetween them. We denote the set of vertices  $(x_1, \dots, x_n)$  of  $W$  as  $V(W)$  and the sequence of edges  $(e_1, \dots, e_{n-1})$  as  $E(W)$  ([need it?](#)).

The vertices  $x_1$  and  $x_n$  are called the *end vertices* of  $W$  and we also say that  $W$  is an  $(x, y)$ -walk. The **length** of  $W$  is defined as the length of the sequence of edges; a walk consisting of only one vertex has length zero. [colon, really?](#)

**Definition 3.5** (Distance). The **distance** of two vertices  $x, y$  in a directed graph  $G$  ([means?](#)), is defined as the minimum length of an  $(x, y)$ -walk, if any such walk exists, otherwise  $\text{dist}(x, y) = \infty$ . In short,

$$\text{dist}(x, y) = \inf\{|E(W)| \mid W \text{ is } (x, y)-\text{walk}\}.$$

$|E(W)|$  is not explained. Necessary?

**Proposition 3.6.** *The distance function  $\text{dist} : V(G) \times V(G) \rightarrow \mathbb{N}$  of a directed graph  $G$  satisfies the triangle equality,*

$$\text{dist}(x, z) \leq \text{dist}(x, y) + \text{dist}(y, z), \text{ for } x, y, z \in V(G).$$

*Proof.* Let  $x, y, z$  be vertices in  $G$ . If either no  $(x, y)$ -walk or  $(y, z)$ -walk exists, the inequality holds by definition. Other wise, let  $W$  be an  $(x, y)$ -walk of minimal length and let  $U$  be a  $(y, z)$ -walk of minimal length. Certainly, by concatenating  $W$  and  $U$  we obtain an  $(x, z)$ -walk of length  $|E(W)| + |E(U)| = \text{dist}(x, y) + \text{dist}(y, z)$ , proofing that

$$\text{dist}(x, z) \leq \text{dist}(x, y) + \text{dist}(y, z).$$

□

More to do:

- summarize category of directed (weighted) pseudographs
- weights!
- vertices will also be called nodes and neurons, edges will also be connections or synapses.
- subgraphs
- ~~vertex set, edge set  $E(G), V(G)$ .~~
- $\omega(e)$  is weight, connection strength or synaptic weight (as a side remark)
- extend to category of weighted directed pseudographs (isomorphisms)
- path
- adjacency matrix
- converses of graph related to opposite category?
- ~~in-and out-degree~~
- ~~triangle inequality for distance,  $\text{dist}(x, z) \leq \text{dist}(x, y) + \text{dist}(y, z)$~~

References for this chapter: <http://nlab.mathforge.org/nlab/show/graph>, <http://nlab.mathforge.org/nlab/show/quiver>, (Bang-Jensen and Gutin 2008)

*focus on labeled,  
simple directed  
graphs*

### 3.3 RANDOM GRAPH THEORY

From this chapter on, as it is common and practical when talking about random graph models, we move away from the abstract notion of graphs and their equivalence classes and consider *labeled graphs*, where the edge set of a graph with  $n$  vertices takes the form  $V = \{1, \dots, n\}$ . Simple directed graphs constitute the fundamental mathematical object underlying the concepts developed in this work and if not specified otherwise, all graphs are assumed to be labeled and simple directed.

The concept of a random graph was first formally introduced by Erdős and Rényi (1959). In their  $G(n, N)$  model, a graph with  $n$  vertices and  $N$  edges is randomly and with equal probability selected from the set of such possible graphs. In the same year Gilbert (1959) independently introduced his  $G(n, p)$  model, realizing edges between vertex pairs with a fixed probability  $p$ . The two models are closely related (Luczak 1990) and overlap in literature, both at times being referred to as *Erdős-Rényi graphs*. Here we focus on the  $G(n, p)$  model, as it closer in concept to a computational implementation of a random graph. Defining it in detail in 3.7, we will refer to the random graph model as the *Gilbert random graph model*.

In general, a random graph model is a probability space over a set of graphs (Janson et al. 2000). Rather than specifying the sample space and probability measure explicitly, random graph models are often defined by a random process that generates such graphs, leaving probability measure and sample space implicit (Bollobás 2001). The term *random graph*, in the graph theoretical context, refers to the random graph model itself. Especially in the computational context however, a random graph often refers to a single graph generated by a random process. Here we try to avoid this ambiguity and strictly refer to the mathematical object as a random graph model.

Keeping in mind that the term *graph* now refers to labeled, simple directed graphs if not otherwise specified we define  $G^n$  to be the set of simple directed graphs with  $n$  vertices,

$$G^n := \{G \mid G \text{ graph}, |V(G)| = n\}.$$

We first introduce Gilbert's random graph model  $G(n, p)$  by explicitly defining a probability space over  $G^n$  and show later how the model may be realized as a random process.

**Definition 3.7** (Gilbert random graph model). Let  $n \in \mathbb{N}$  and  $0 \leq p \leq 1$ . The *Gilbert random graph model*  $G(n, p)$  is a discrete probability space over  $G^n$  with event space  $\mathcal{P}(G^n)$  and probability measure  $P$ ,

such that every graph  $G$  with  $|E(G)| = k$  edges appears with equal probability

$$P(G) = p^k(1-p)^{n(n-1)-k},$$

for  $0 \leq k \leq n(n-1)$ .

*Remark.* Clearly  $G(n, p)$  is well-defined, as there exist  $\binom{n(n-1)}{k}$  distinct labeled graphs with  $n$  vertices and  $k$  edges and thus

$$\sum_{G \in G^n} P(G) = \sum_{k=0}^{n(n-1)} \binom{n(n-1)}{k} p^k (1-p)^{n(n-1)-k} = 1,$$

after the binomial theorem.

Equivalently, the Gilbert random graph model can be defined as a stochastic process; to an empty graph with  $n$  vertices, for each of the  $n(n-1)$  vertex pairs an edge is added at random and independently with probability  $p$ . The probability to obtain a specific graph  $G$  with  $k$  edges is then obviously  $p^k(1-p)^{n(n-1)-k}$ , already proofing the equivalence, since assuming a process as above with edge probability  $p'$  such that the induced probability measure on  $G^n$  equals  $P$  from 3.7, already yields  $p = p'$  in the choice of  $n = 2$  and  $k = 1$ .

equivalent  
definition as  
random process

**Proposition 3.8.** *In- and out-degree distribution of vertices in the Gilbert random graph model are binomial.*

*Proof.* Let  $X$  be a random variable on the random graph model, mapping to the in-degree (out-degree)  $d_G(v)$  of a vertex  $v$  of a graph  $G \in G^n$ . There are  $n-1$  other vertices that, with probability  $p$ , project to  $v$  (receive input from  $v$ ), thus

$$P(X = k) = \binom{n-1}{k} p^k (1-p)^{n-1-k},$$

showing that  $P^X = \mathcal{B}_{n-1,p}$ . □

The Gilbert random graph model is therefore also often referred to as *binomial random graph*. As typical neuronal networks are large ( $n \geq 10^3$ ) with sparse connectivity ( $p \approx 0.1$ ), in- and out-degree distribution can be approximated by a Poisson distribution,  $P^X(k) \approx \text{Pois}_\lambda(k)$ , with  $\lambda = (n-1)p$ , after the Poisson limit theorem.

Most results in the study of random graph models consider  $n \rightarrow \infty$ . In this study we are mostly interested in patterns of connectivity that arise in local circuits, leaving behind limit considerations and employ the Gilbert random graph model as a reference for the development of more detailed and specific random graph models.

### 3.4 GEOMETRIC GRAPHS

The theory of geometric graphs address the embedding of graphs in  $\mathbb{R}^d$ . Planar graphs are graphs that can be drawn on a surface with their edges drawn as straight lines between the vertices, such that no two lines intersect (Diestel 2000). Here we are interested in graphs embedded on surface. In the models introduced, connectivity then depends on geometric properties, such as distance between nodes or relative orientation between vertices. The basic graph type to allow for such connectivity rules is a geometric graph.

**Definition 3.9** (Geometric directed graph). A *geometric directed graph*  $G_\Phi$  is a directed graph  $G$  paired with a map

$$\Phi : V(G) \rightarrow [0, 1]^2,$$

representing vertex positions on the unit square.

This definition diverges from the usual notion of a geometric graph, which determines the existence of edges only between nodes within a spatial distance  $x$  in a specified norm (Penrose 2003). Moreover, geometric graphs are usually only discussed in the context of random graph models, a concept first introduced by Gilbert (1961). Denote the set of geometric graphs with  $n$  edges by  $G_\Phi^n$ . The spatial embedding of geometric graphs allows us to define (random) connectivity depending on vertex positions and inter-vertex distances. Central to this study is the distance-dependent random graph model, in which edges are added with probability  $p(x)$  depending on the distance  $x$  between vertex pairs:

**Definition 3.10** (Distance-dependent random graph model). Let  $n \in \mathbb{N}$  and  $C : [0, \sqrt{2}] \rightarrow [0, 1]$  a continuous map. A *distance-dependent geometric random graph model*  $G_\Phi(n, C)$  is a random graph model over  $G_\Phi^n$ , generated by distributing uniformly at random the  $n$  vertices on the unit square and adding an edge from  $v$  to  $w$  for each vertex pair  $(v, w) \in V(G_\Phi)^2 \setminus \Delta_{V(G_\Phi)}$  with a probability  $C(x)$ , depending on the distance  $x = \|\Phi(v) - \Phi(w)\|$  between the vertices.

We call the function  $C$  the graph's *distance-dependent connection probability profile*. Clearly, connectivity statistics in the distance-dependent graph model intrinsically depend on the choice  $C$ . To develop a thorough understanding of connectivity in the model however, mapping the distribution of inter-vertex distances is equally important. Here we calculate the distribution of the distance between two random points in a square of side-length  $s$ . Being able to identify distributions of transformed random variables is integral to the calculation:

**Lemma 3.11.** Let  $X, Y$  be independent continuous random variables with values in  $\mathbb{R}$ , denote with  $f_X$  and  $f_Y$  their probability distribution functions.

- (1) The distribution of the random variable  $X + Y$  is given by the probability density function

$$f_{X+Y}(x) = \int_{\mathbb{R}} f_X(z)f_Y(z-x) dz.$$

- (2) The distribution of the random variable  $X^2$  is given by the probability density function

$$f_{X^2}(x) = \begin{cases} \frac{1}{2\sqrt{x}} (f_X(\sqrt{x}) + f_X(-\sqrt{x})) & x > 0 \\ 0 & x \leq 0 \end{cases}$$

- (3) Let  $X$  only take positive values. Then the distribution of the random variable  $\sqrt{X}$  is given by the probability density function

$$f_{\sqrt{X}}(x) = \begin{cases} 2x f_X(x^2) & x \geq 0 \\ 0 & x < 0 \end{cases}$$

**Theorem 3.12.** Let  $D$  be a random variable mapping to the distance of two random points in the square  $[0, s]^2$  of side-length  $s$ . Then the distribution of  $D$  is given by the probability density function

$$f(x) = \begin{cases} \frac{2x^4 - 8sx^3 + 2\pi s^2 x}{s^4} & x \in [0, s] \\ \frac{H(x)}{s^4} & x \in [s, s\sqrt{2}), \\ 0 & x \notin [0, s\sqrt{2}) \end{cases} \quad (3.1)$$

where

$$H(x) = 8sx\sqrt{x^2 - s^2} - 2x^3 - 4s^2x \left( 1 + \arcsin \left( 1 - \frac{2s^2}{x^2} \right) \right).$$

*Proof.* We follow the approach described by Moltchanov (2012). Consider two independently and uniformly distributed random points  $p_1 = (x_1, y_1)$  and  $p_2 = (x_2, y_2)$  in  $[0, s]^2$ . The distance between  $p_1$  and  $p_2$  is given as

$$\|p_1 - p_2\| = \sqrt{(x_1 - x_2)^2 + (y_1 - y_2)^2}.$$

As a first step we calculate the distribution for  $\Delta_x = x_1 - x_2$ . Denote with  $f_{\Delta_x}$  its probability density. Then, since  $f_{-x_2}(z) = f_{x_2}(-z)$ ,

$$f_{\Delta_x}(d) = f_{x_1 + (-x_2)}(d) = \int_{\mathbb{R}} f_{x_1}(z)f_{x_2}(z-d) dz \quad (3.2)$$

after Lemma 3.11. Density functions for  $x_1$  and  $x_2$  are given by

$$f_{x_1}(z) = f_{x_2}(z) = \begin{cases} \frac{1}{s} & \text{for } z \in [0, s] \\ 0 & \text{otherwise.} \end{cases}$$

Thus we may only obtain non-zero values in (3.2) for  $d \in (-s, s]$ , as otherwise either one of the factors in the integrand is zero. In full we obtain the triangular distribution (Simpson 1755),

$$f_{\Delta_x}(d) = \begin{cases} 0 & d \notin (-s, s] \\ \frac{s+d}{s^2} & d \in (-s, 0] \\ \frac{s-d}{s^2} & d \in (0, s]. \end{cases}$$

Next we calculate the distribution for  $\Delta_x^2 = (x_1 - x_2)^2$ . Using Lemma 3.11 once again we obtain for  $d > 0$

$$\begin{aligned} f_{\Delta_x^2}(d) &= \frac{1}{2\sqrt{d}} \left( f_{\Delta_x}(\sqrt{d}) + f_{\Delta_x}(-\sqrt{d}) \right) \\ &= \frac{1}{2\sqrt{d}} \left( \frac{s - \sqrt{d}}{s^2} + \frac{s + (-\sqrt{d})}{s^2} \right) = \frac{1}{s\sqrt{d}} - \frac{1}{s^2}, \end{aligned}$$

and  $f_{\Delta_x^2}(d) = 0$  for  $d \leq 0$ . Note that of course,  $f_{\Delta_x^2} = f_{\Delta_y^2}$  and we will refer to this density function as  $f_{\Delta}^2$ . Convolution yields again the probability density function for the sum of the random variables  $\Delta_x^2$  and  $\Delta_y^2$ ,

$$f_{\Delta_x^2 + \Delta_y^2}(d) = \int_{\mathbb{R}} f_{\Delta^2}(z) f_{\Delta^2}(d-z) dz.$$

Finally Lemma 3.11 lets us compute

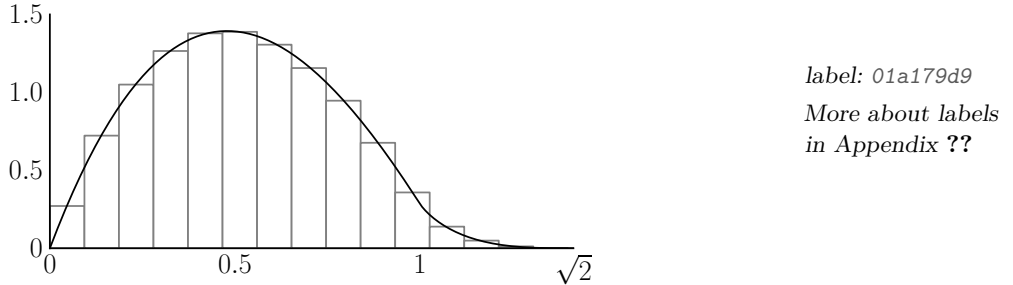
$$f_D(d) = f_{\sqrt{\Delta_x^2 + \Delta_y^2}}(d) = 2d f_{\Delta_x^2 + \Delta_y^2}(d^2),$$

for  $d \geq 0$ , yielding expression (3.1) for probability density function of  $D$  (Mathematica A.1, A.2).  $\square$

The distribution for the distance between two random points in the unit square  $[0, 1]^2$ , is then obtained from (3.1) by setting  $s = 1$ . The probability density function  $f$  becomes

$$f(x) = \begin{cases} 2x^3 - 8x^2 + 2\pi x & x \in [0, 1) \\ 8x\sqrt{x^2 - 1} - 2x^3 & x \in [1, \sqrt{2}) \\ -4x - 4x \arcsin\left(1 - \frac{2}{x^2}\right) & x \in [\sqrt{2}, 1] \end{cases} \quad (3.3)$$

Plotting  $f$  in combination with the results of a numerical simulation (10000 points randomly distributed on unit square, extracted distances binned to a of width  $\sqrt{2}/15$ ) verifies our calculation:



Density functions 3.1 and 3.3 are of high importance. Here we use 3.3 to compute the probability that a random pair of vertices in the distance-dependent random graph model is connected:

**Corollary 3.13.** *Let  $v \neq w$  be vertices in an arbitrary realization of  $G_\Phi(n, C)$ . The probability  $p$  for an edge from  $v$  to  $w$  is given by*

$$p = \int_0^{\sqrt{2}} C(x)f(x) dx,$$

where  $f(x)$  is the probability density function (3.3).

**Example** Let  $C(x) = 1 - \frac{x}{\sqrt{2}}$ . Then we compute the probability to find an edge between a random vertex pair in  $G_\Phi(n, C)$  according to Theorem 3.13 as

$$p = \int_0^{\sqrt{2}} f(x) dx - \frac{1}{\sqrt{2}} \int_0^{\sqrt{2}} x f_D(x) dx = 1 - \frac{1}{\sqrt{2}} \mathbf{E}[D].$$

The expected distance between two random points on the unit square is computed as  $\mathbf{E}[D] \approx 0.521405$  ([Mathematica A.1](#)), a result confirmed by [Philip \(2007\)](#). Thus we obtain the probability for connection of  $p \approx 0.631311$



# 4

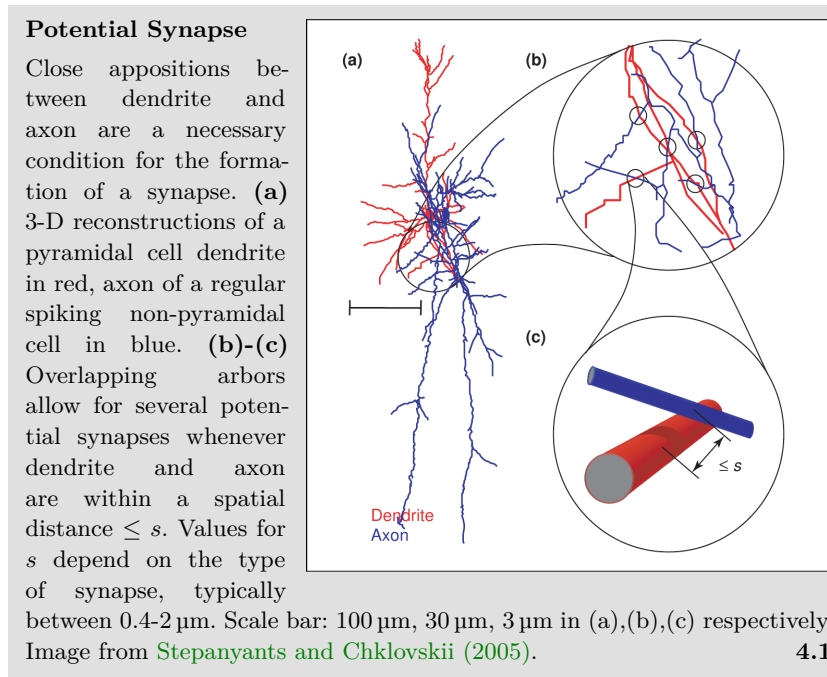
## NETWORK MODEL

---

Referring to anisotropic characteristics in local cortical circuits of the rat's brain, a network model implementing anisotropic tissue geometry is developed. The introduction of a rewiring algorithm and qualitative anisotropy measure lay the foundation for the analysis of structural aspects of this model in Chapter 5.

#### 4.1 ANISOTROPY IN NEURAL CONNECTIVITY

Neurogeometry addresses the problem of inferring synaptic connectivity from the geometric shapes of axon and dendrites. A fundamental concept in this field is that of a *potential synapse* (Stepanyants et al. 2002). Defined as the potential axonal-dendritic connection of two neurons, present whenever the axon of one neuron is within a spatial distance  $s$  of the dendrite of the other, it is a necessary, although not sufficient, condition for the formation of a synaptic connection (Figure 4.1). The existence of such close appositions solely depends on dendritic and axonal anatomy; identification of defining morphological characteristics in both axon and dendrite would therefore allow for a model of local network connectivity, assuming for example that a certain ratio  $r$  of potential synapses turn into active contacts independently. It is the hope that such a model, motivated from the geometry of a neuron's functional compartments, not only displays inherent patterns of connectivity similar to what has been observed in biological networks, but also proofs itself as a testing ground for how this connectivity may affect network dynamics.



high variability in  
axonal  
morphology

Finding stereotypical anatomical characteristics however is difficult, as axonal morphology is, in general, highly diverse (Debanne 2004). Across different species, distinct regions in the central nervous system and different neuron types, axons display a wide variety of shapes characterized by morphometric parameters such as total length, branching complexity and axonal extent (Ropireddy et al. 2011). Typical exam-

ples of distinct morphology include the T-shaped axons of cerebellar granule cells branching only at a singular point (Ramon and Cajal 1911), and axons of hippocampal CA3 pyramidal cells, which, in stark contrast, may feature up to 40 branches resulting in a total length of axon collaterals of up to 12 mm (Ishizuka et al. 1990).

It is therefore imperative to confine this analysis to a specific brain region and neuron type. In this study, we set the focus on circuits of pyramidal cells in the mammalian cortex. More specifically, local circuits of thick tufted layer V pyramidal neurons in the rat's somatosensory cortex have been the target of advanced experimentation (Song et al. 2005; Perin et al. 2011; Romand et al. 2011; Ramaswamy et al. 2012), and will serve as a benchmark for results in neural morphology and network connectivity in this report.

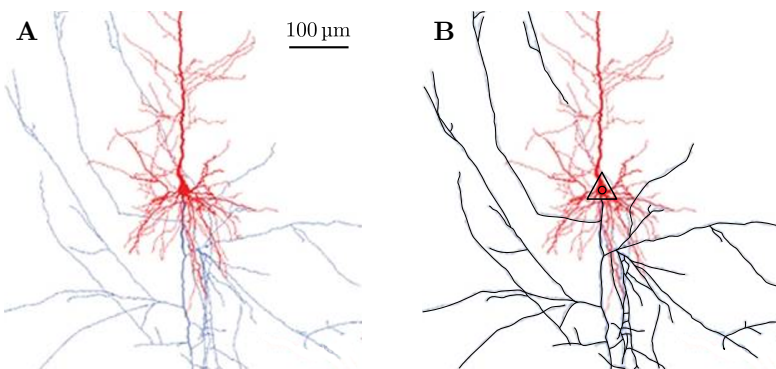


**Figure 4.2: Tracing axonal branching of a pyramidal cell** In a 3-D model reconstructed from biocytin-labeled thick-tufted layer V pyramidal cells in the somatosensory cortex of postnatal (day 14) Wistar rats, Romand et al. (2011) depict dendritic compartments in red, axonal compartments in blue. **A)** A 600  $\mu\text{m}$  window centered on the soma of the pyramidal cell shows the main stem of the cell's axon projecting downwards in a straight line, collaterals branching at various angles. **B)** Using image manipulation software, axon morphology was manually traced and is emphasized in black.

Axonal morphology of pyramidal cells in the cerebral cortex is well described. From the soma the single main stem of the axon originates and projects downwards, describing a trajectory closely resembling a straight line (Braitenberg and Schüz 1998). At arbitrary points along this path, collaterals branch off at various angles and constitute themselves linear paths until they further ramify or terminate. Displaying a high degree of ramification, axonal trees of cortical pyramidal cells build, in general, complex structures (Petersen et al. 2003; Ramaswamy et al. 2012). Cortical slice experiments analyzing neural anatomy are typically constrained by a slice thickness of 300  $\mu\text{m}$ . On this scale, 3-D reconstruction from labeled thick tufted layer V pyramidal cells reveals

cortical axons  
form straight lines,  
arborize profusely

characteristic morphology of the axonal tree (Figure 4.2). The downwards projecting, straight axon branches at several points, forming collateral branches that travel in linear path as well.

In a statistical view, this characteristic axonal morphology results in high axon branch densities along the main stem, whereas distant regions display a relatively low density (Figure 4.3). Specifically, axon collaterals do not cluster around the soma but align with the main stem's projection. As presence of an axonal branch constitutes a necessary condition for a potential synapse, a higher concentration of potential and, subsequently, realized synapses is expected in regions of high branch density. For a coherent picture of local connectivity profiles, however, dendritic morphology needs to be considered as well.

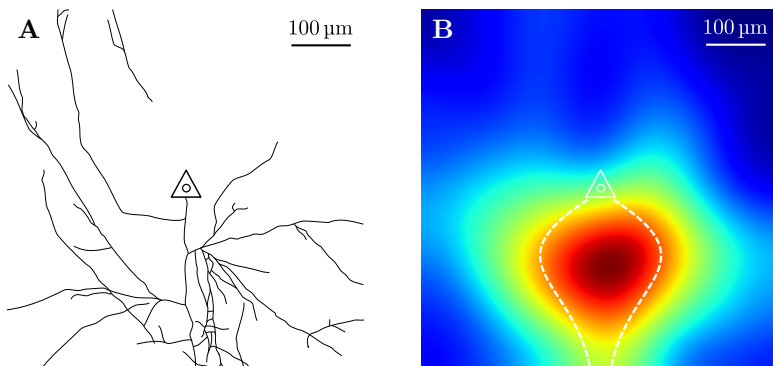


**Figure 4.3: Illustrating axonal branch density** In a sample of 5 reconstructions from thick-tufted layer V pyramidal cells (Romand et al. 2011), tracing axonal morphology illustrates characteristic branch density along the axon's main stem. **A)** Example of extracted axonal tree. Outline manually traced using image manipulation software. Soma indicated by triangle. Original data from Romand et al. (2011). **B)** Overlaying 5 axonal trees extracted as in A), applying a Gaussian filter and displaying high axon densities in warm colors, illustrates the characteristic higher branch densities along the axon's main stem.

*basal dendrites dominate local connectivity*

Dendritic anatomy of cortical pyramidal cells is inherently bipartite. From the soma several *basal dendrites* emerge and extend into arbitrary directions, branching profusely until they terminate. The single *apical dendrite* emerges from the apex of the pyramidal cell and ascends in a linear trajectory, forming occasional collateral branches until finally terminating into the apical tuft, where the dendrite branches several times to form a tree like structure (Feldman 1984). On the scale of typical cortical slice thickness, however, the apical dendrite is cut off and the basal dendrite dominates the dendritic morphology and potential of dendritic-axonal connections (Figure 4.4). The radial extension of dendritic branches results in a high concentration of dendritic branches

around the soma, much in the contrast to the findings of axonal branch densities before.

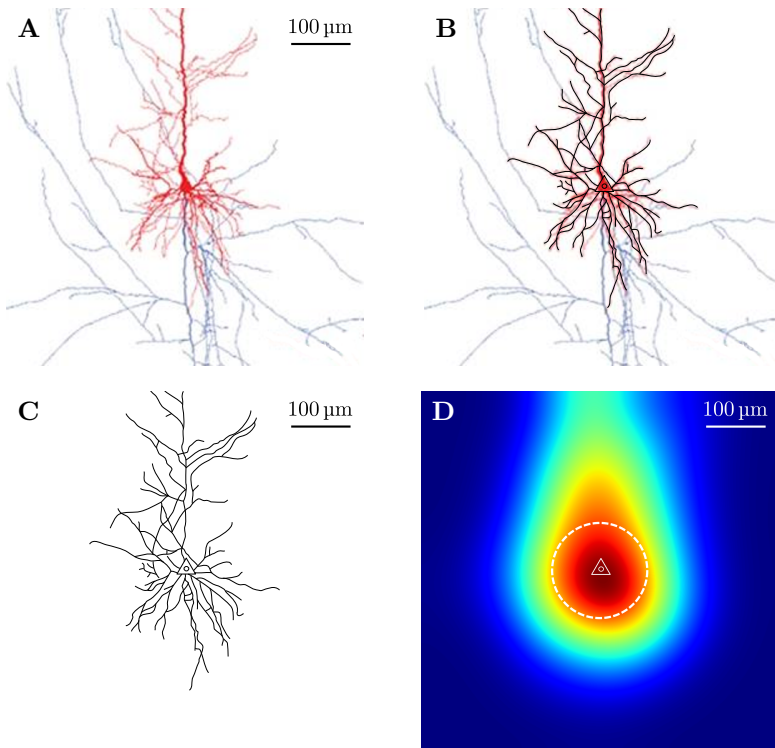


**Figure 4.4: Dendritic morphology and branch density** Using neuronal morphology of thick-tufted layer V pyramidal cells recorded by Romand et al. (2011), dendritic anatomy is traced and combined to illustrate high branch density around the soma. **A)** In a 600  $\mu\text{m}$  window centered on the soma, basal dendrites (red) are visible extending around the soma. The ascending thick apical dendrite (red) is cut off and apical tuft is not shown. **B)-C)** Manual tracing of dendritic outlines in five samples (one shown), allows for clearer identification of stereotypical morphology and later analysis. **D)** Combining 5 dendritic outlines as shown in C) and subsequent Gaussian filtering reveals the relatively high dendritic branch density around the soma.

Combining the above results of dendritic and axonal branch densities in the light of neurogeometry, a clear concept of anisotropy of neural connectivity emerges. As dendritic branches of potential post-synaptic targets extend radially from the soma and do not display a preferred direction, target neurons for outgoing synaptic contacts originating from a single pyramidal cell, cluster around the downwards projecting axon (Figure 4.5). In their in-depth study, Stepanyants and Chklovskii (2005) confirm the overrepresentation of potential synapses along the axon for pyramidal cells. Consistent with the notion that stereotypical morphology of pyramidal cells is intrinsic to the local network's connectivity

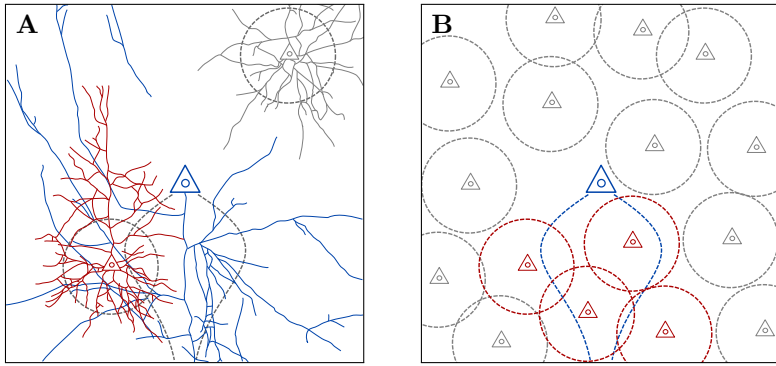


**Figure 4.5: Connected neurons of a single pyramidal cell align with axonal projection** Reducing the full axonal (blue, cf. Figure 4.2) and dendritic trees (red, gray, cf. Figure 4.4) as shown for two neurons in A) to their stereotypical axonal (blue) and dendritic profiles (red, gray) in B), demonstrates how connected neurons (red) tend to cluster around the pre-synaptic axon's profile, as spatial closeness constitutes a necessary condition for the formation of contacts. Unconnected neurons (gray) are found distant from the axon's projection, but not necessarily distant from the soma.

profile, they also find that anisotropy of this degree is *not* present in spiny stellate neurons located in lower-layer-4.

## 4.2 ANISOTROPIC GEOMETRIC NETWORK MODEL

Taking up the concept of anisotropy in neural connectivity introduced in the last section, we propose here, as basis for this study, a simple geometric network model featuring anisotropic connectivity. Constructing such a model, we're challenged with resembling the anisotropic aspects outlined last section as closely as possible, while at the same time making the model as simple and as abstract as possible, to allow for an abstract and analytical study of such anisotropic networks.

With this in mind, we propose the following model: On a square surface of side length  $s$ , a number of  $N$  point neurons are randomly, uniformly distributed. Connected neighbors are then calculated for each neuron separately and independently, by determining the randomly, uniformly distributed direction of the neuron's single axon. In this direction the axon traverses over the surface describing a straight path, terminating only when an edge of the surface is reached. Directed contacts are made with every neuron that is within a width  $w(x)$  of the axon's trajectory, where in general  $w$  depends on the axon length  $x$  at this point (Figure 4.6).

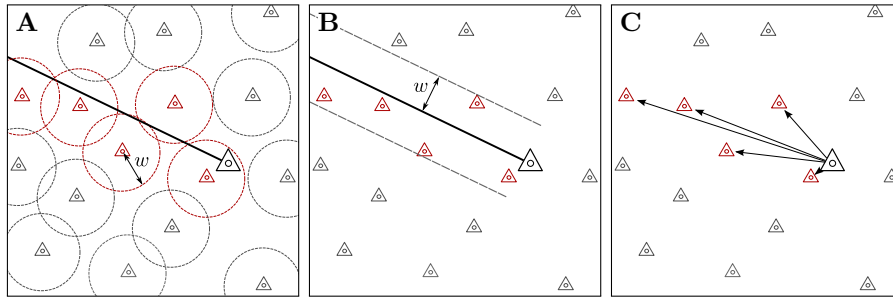


**Figure 4.6: Anisotropic geometric network model and interpretations of width parameter  $w$**  Illustrating the process of finding connections for one neuron (large triangle, black), the axon describes a linear trajectory in an arbitrary direction and until terminating on the surface's edge. Target neurons (red) are encountered along the path within a (here constant) distance  $w$ , which is in **A**) interpreted as a dendritic radius or, equivalently, in **B**) as a “bandwidth” of the axon. Connections to the encountered targets are then established as projections in **C**), consistent with the directed nature of synapses in biological networks (cf. Chapter 2).

The implementation of arbitrary axonal orientation is crucial to the model. Although cortical axons are described as consistently projecting downwards (Braitenberg and Schüz 1998, cf. Section 4.1), combining exclusively vertically aligned axons with the simplified axonal and dendritic morphological profiles would result in a “vertically staggered

random axonal orientation yields relevant connectivity

connectivity" - neurons could then only project to targets located below them. It is in fact not a vertical alignment of axon orientation, but the anisotropy in neural connectivity - the observation of neuronal targets aligning with the axonal projection - that we try to capture and analyze in this model.

We will refer to the model as the *anisotropic geometric network model*. Trying to provide a simple, abstract model isolating anisotropy in connectivity, in most of this study the width  $w(x)$  is assumed to be constant,  $w(x) = w$ , a notable exception being the exploration in ???. In the graph theoretic context the anisotropic network model is a random graph model, in which a realization of the random process results in a geometric directed graph with a special mode of connectivity. We can formally define such realization as:

**Definition 4.1** (Anisotropic geometric graph). Let  $n \in \mathbb{N}$  and  $w \in (0, \infty)$ . An *anisotropic geometric graph*  $G_{n,w}$  then consists of a tuple  $(G, \Phi, a)$ , of a simple directed graph  $G$  with  $|V(G)| = n$  vertices and the maps  $\Phi : V(G) \rightarrow [0, 1]^2$  and  $a : V(G) \rightarrow [0, 2\pi)$ , such that for every vertex pair  $v, v' \in V(G)$  and edge  $e \in E(G)$  with  $s(e) = v$  and  $t(e) = v'$  exists if and only if the inequalities

$$R_{-a(v)} (\Phi(v') - \Phi(v)) \hat{e}_x \geq 0 \quad \text{and} \quad \left| R_{-a(v)} (\Phi(v') - \Phi(v)) \hat{e}_y \right| \leq \frac{w}{2}$$

hold. Here  $R_\varphi$  is the rotation matrix of angle  $\varphi$  in the Cartesian plane and  $\hat{e}_x, \hat{e}_y$  are the standard unit vectors.

The anisotropic random graph model then is then giving the probability distribution over the set of anisotropic random graphs by describing a random process generating such graph.

**Definition 4.2** (Anisotropic random graph model). Let  $n \in \mathbb{N}$  and  $w > 0$ . The *anisotropic random graph model*  $G(n, w)$  is a probability space over the set of anisotropic geometric graphs with a probability distribution induced by the following process: Let  $G$  be an empty graph with  $n$  vertices. Assign randomly and uniformly to every vertex  $v \in V(G)$  a position  $\Phi(v) \in [0, 1]^2$  and axonal orientation  $0 \leq a(v) < 2\pi$ . Then add edges such that  $(G, \Phi, a)$  is an anisotropic geometric graph  $G_{n,w}$ .

*anisotropic model  
is scale-free*

As with every geometric graph model introduced, we restrict the surface to be the unit square. This does not limit the model, as only the relative width of the axon band in regard to the surface's side length is determining connectivity statistics - the expected number of connections is easily obtained by the quotient of the area covered by the axon and the surface area, making connectivity statistics in the anisotropic random graph model scale-free.

The following maybe interpreted as a study of anisotropic geometric graphs in the light of a neuroscientific context. To enable such an analysis, a few more concepts are needed. The introduction of those concepts composes the rest of the chapter. A first important step is the numerical implementation of the anisotropic network model.

### 4.3 NUMERICAL IMPLEMENTATION

Numerical implementation of the anisotropic random graph model was achieved in Python<sup>1</sup>. Relying on NumPy as part of the scientific Python library SciPy<sup>2</sup> for the more complex mathematical computations, the implementation also uses graph-tool<sup>3</sup>, to ensure convenient and efficient handling of the created networks.

The algorithm for the generation of anisotropic networks closely resembles Definition 4.1. After randomly distributing  $N$  neurons on the square of side-length  $s$ , for every neuron a random axon orientation  $a \in [0, 2\pi)$  is chosen and an affine transformation, such that the current neuron is located at the origin and its axon projection aligns with the positive x-axis, secures a straightforward implementation of connectivity, using the the inequalities in Definition 4.1 as a rule for establishing connections.

To harness the numerical implemenation to generate networks, a set of parameters needs to be chosen. The network size  $N$  strongly influences the needed computational efforts in calculations based on the generated graphs and has thus been set to  $N = 1000$ . Choosing the surface side-length arbitrarily as  $s = 100$ , the axon width  $w$  determines connectivity in the network, the relation between width  $w$  and overall connection probability  $p$  being shown in Figure 4.7. In their analysis of connectivity of thick-tufted layer V pyramidal cells in neonatal rats (day 14), Song et al. (2005) report an overall connection probability of  $p = 0.116$ , consistent with prior reports of a cortical connection probability of  $p \approx 0.1$ . Choosing  $w$  to be constant, we determine the axon width such that overall connectivity matches the value report by Song et al. and obtain  $w/2 = 12.6$  (Figure 4.7).

*parameter set  
chosen to resemble  
cortical circuits*

Having determined a suitable set of parameters as  $N = 1000$ ,  $s = 100$  and  $w = 25.2$ , we generate 25 graphs with this parameter set

<sup>1</sup> Python Software Foundation. Python Language Reference, version 2.7. Available at <http://www.python.org>

<sup>2</sup> Eric Jones, Travis Oliphant, Pearu Peterson and others. NumPy version 1.6.1. Available at <http://www.scipy.org>

<sup>3</sup> Tiago P. Peixoto. Efficient network analysis. Version 2.2.18. Available at <http://graph-tool.skewed.de/>

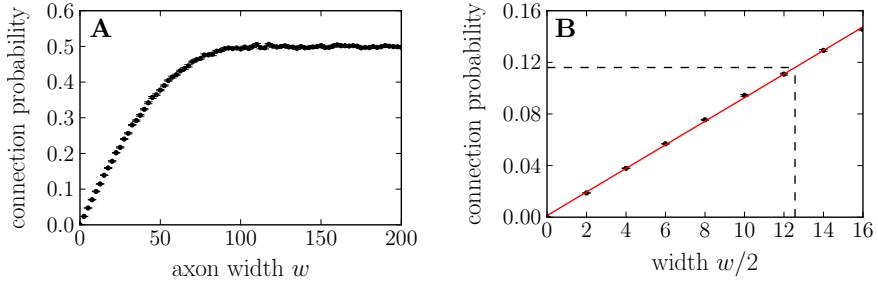


**Figure 4.7: Axon width dependent connection probability determines parameter for numerical analysis** Generating anisotropic networks with different axon widths  $w$  and extracting probability  $p$  of directed connection between two random nodes, demonstrates the dependency of  $p$  on the width parameter  $w$ . **A)** At an axon width of over  $w = 100$ , exceeding the square's side length, the connection probability saturates at  $p = 0.5$ , as axon bands are essentially “cutting” the square in a connected and unconnected half (c5b64f3e). **B)** For small  $w$  the connection probability is a linear function of  $w$ , allowing the width  $w_S/2$  at which  $p(w_S) = 0.116$  to be determined by a linear fit as  $w_S/2 = 12.6$  (585a946f).

sample graphs as  
reference for  
structural analysis

(label: N1000w\_ax126-flat\_graph0-24). This set of sample graphs will serve as a reference for the following structural analysis. Extending the set by the (partially) rewired sample graphs (see Section 4.5) and by purely distance-dependent graphs best resembling the anisotropic networks (see Section 4.4) we obtain a resourceful reference for the analysis of structural features of anisotropic geometric graphs, that we will frequently employ to obtain quantitative and qualitative results.

#### 4.4 DISTANCE DEPENDENT CONNECTIVITY

In Gilbert's random graph model  $G(n, p)$ , probability of connection  $p$  is independently chosen and a fixed value for all vertex pairs. The anisotropic geometric graph model introduced in Section 4.2 is itself a random graph model - node positions as well as preferred directions of connection are uniformly at random distributed. In contrast to Gilbert's model however, neither is the probability of connection between a given vertex pair independent of the realization of other edges in the graph, nor is it a fixed value - probabilities strongly depend on internode distance in the anisotropic geometric graph model introduced.

*random graph  
models in  
Section 3.3*

Analyzing dependencies in the anisotropic model, specifically by identifying prevalent patterns of connectivity and relating these modes of non-randomness to biological findings, is the main focus of Chapter 5. However, such structural correlations may not necessarily be an inherent feature of the network's anisotropy - distance dependent connectivity alone, as imposed by the model's specific geometry, may be the cause for emerging dependencies. It is therefore a crucial initial task to map the anisotropic model's distance dependent connection probability. Inferring connection probability as a function of internode distance and comparing it with computational results, in this section we explore distance connectivity of the anisotropic network model, securing a vital component in the analysis of structural features.

**Theorem 4.3.** *Let  $(G, \Phi, a)$  represent an arbitrary realization of the anisotropic random graph model  $G(n, w)$ . Define  $C : [0, \sqrt{2}] \rightarrow [0, 1]$  as the distance-dependent connection probability profile of  $(G, \Phi)$ , that is such that  $C(x)$  is the probability that for a vertex pair  $(v, v') \in V(G)^2 \setminus \Delta_{V(G)}$  in distance  $x = \|\Phi(v) - \Phi(v')\|$  the vertex  $v$  projects to vertex  $v'$ . Then*

$$C(x) = \begin{cases} \frac{1}{2} & \text{for } x \leq w/2 \\ \frac{1}{\pi} \arcsin\left(\frac{w}{2x}\right) & \text{for } x > w/2. \end{cases}$$

*Proof.* Let  $v, v'$  be a pair of vertices in  $V(G)^2 \setminus \Delta_{V(G)}$  in Euclidean distance  $x$  of each other. The vector difference  $\Phi(v') - \Phi(v)$  may then be written as  $xe^{i\theta}$ , with  $0 \leq \theta < 2\pi$ . We have

$$R_{-\alpha(v)} xe^{i\theta} = xe^{i(\theta - \alpha(v))}.$$

Only for suitable combination of  $\theta$  and  $\alpha(v)$  an edge from  $v$  to  $v'$  exists. Assuming  $\alpha(v)$  fixed, we calculate the probability of connection depending on the random choice of  $\theta$ . We can assume  $\alpha(v) = 0$ , otherwise the same argument holds for  $\theta' = \theta - \alpha(v)$ .

From 4.1 we obtain the necessary and sufficient conditions

$$x \cos \theta \geq 0 \quad \text{and} \quad |x \sin \theta| \leq \frac{w}{2}.$$

Choosing uniformly at random  $\theta$  in the range of  $[0, 2\pi)$ , the first condition is satisfied with a probability of  $\frac{1}{2}$ . Consider for the second condition  $\theta \in [0, \pi)$ . We have

$$\sin \theta \leq \frac{w}{2x},$$

and for  $x \leq \frac{w}{2}$  the inequality holds for all  $\theta$  by definition of  $\sin \theta$ . In the case of  $x > \frac{w}{2}$ , we note that for the first condition to hold  $\theta$  must already be in  $[0, \frac{\pi}{2})$  and can thus write the second condition  $\theta$  as

$$\theta \leq \arcsin \frac{w}{2x},$$

yielding  $C(x)$  by combining the considerations above and using the symmetry of sine for  $\theta$  in the third and fourth quadrant.  $\square$

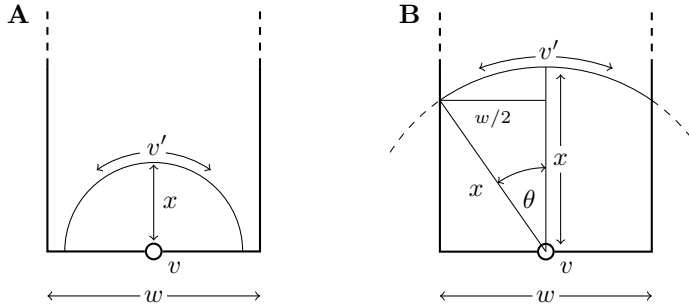


**Figure 4.8: Illustrating the proof of Theorem 4.3** Distance-dependent connectivity profile  $C(x)$  in an anisotropic geometric graph calculated from geometric dependencies. **A)** In the case of  $x \leq w/2$ , target  $v'$  may be located anywhere on the shown semicircle and therefore receives input from  $v$  with probability  $1/2$ . **B)** For  $x > w/2$ , suitable positions for target  $v'$  are dependent on  $x$ . The geometric relation  $\sin \theta = w/2x$  leads to the distance-dependent connectivity profile as described in Theorem 4.3.

distance-dependent sample graphs as reference

We can verify this result by extracting the distance-dependent connection probabilities in the sample graphs created in Section 4.3. Combining data of all 25 graphs, we find that connection probabilities perfectly match the theoretical prediction (Figure 4.9). Additionally we're able to extend the reference sample graphs by distance-dependent networks (Definition 3.10). Using Theorem 4.3 in conjunction with the sample graph parameter set ( $N = 1000$ ,  $s = 100^4$ ,  $w = 25.2$ ) we easily obtain the expected distance-dependent connectivity profile for the

<sup>4</sup> The generalization of Theorem 4.3 to allow for arbitrary side-length  $s$  is trivial and omitted here

created sample graphs and, using this profile, generate purely distance-dependent networks<sup>5</sup>. Being highly interested in structural features not explained by distance-dependent connectivity, the numerical analysis in this work will heavily rely on these networks to identify aspects that are inherent to the anisotropy in connectivity.

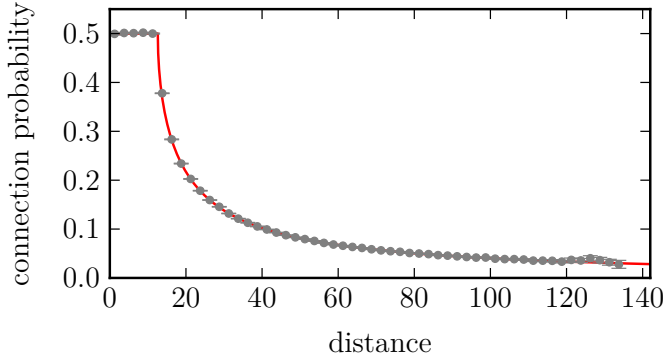


**Figure 4.9: Predicted distance-dependent connection probability profile is matched by numerical results** Averaging distance-dependent connection probabilities over the 25 sample graphs, we find the expected profile calculated in Theorem 4.3 is matched perfectly by the numerical results. (dbffa88e)

## 4.5 REWIRING

It is in our highest interest to compare results to. To this end we introduce an algorithm that preserves distance-dependent connectivity as found in Proposition ??, but eliminates anisotropy in network connectivity by consecutively rewiring existing connections to new suitable targets.

*eliminate  
anisotropy  
through rewiring*

Rewiring as presented here, will provide the transition from anisotropic connectivity to networks isotropic in connectivity, closely resembling purely distance-dependent networks. Applying this process only partially will then allow us to analyse structural features as they change with a varying degree of isotropy, asserting the importance of this process to our study.

In designing the specific rewiring algorithm we identify two requirements that our implementation should satisfy:

1. elimination of anisotropy in connectivity
2. preservation of distance-dependent connectivity

---

<sup>5</sup> label: N1000-dist\_depend-flat\_graph-00-24.xml.gz

The second point is especially important to us, as we want to impose isotropy on the network at “minimal cost”, that is by changing as little as possible about the other characteristics of the network’s connectivity. The following process respects both of the points above: For every edge between vertices  $v$  and  $v'$  with inter-vertex distance  $x$ , identify neurons with distance to  $v$  in the range of  $(x - \varepsilon, x + \varepsilon)$  as potential new targets. Then pick at random one of these vertices, including  $v'$ , as a new target for the current edge, if such an edge doesn’t already exist ([Figure 4.10](#)). In the graph theoretic context we formally define a rewiring as follows:

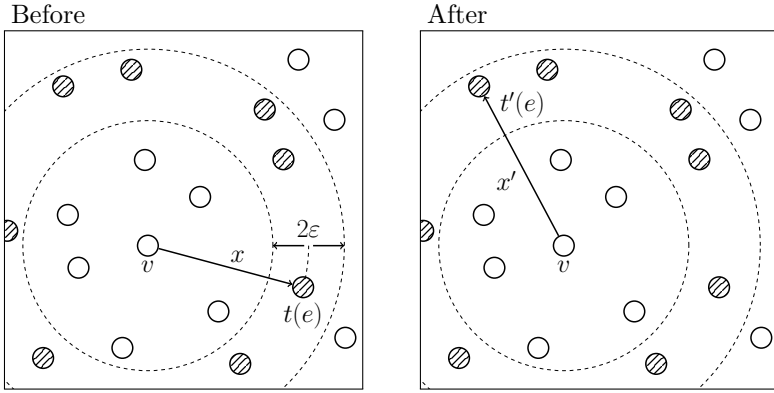


**Figure 4.10: Rewiring transforms anisotropic geometric graphs to networks with isotropic connectivity** For a given edge  $e$  with a distance  $x$  from its source vertex  $v$  to its target vertex  $t(e)$ , potential new targets (striped) are found in within a distance  $(x - \varepsilon, x + \varepsilon)$  of  $v$ . The rewired edge then projects from  $v$  to a new target  $t'(e)$ , randomly chosen from the set of vertices within in this range. Inter-vertex distance between  $v$  and  $t'(e)$  differs by less than  $\varepsilon$  from  $x$ , ensuring that for small  $\varepsilon$  the original distance-dependent connectivity is preserved. (Note that all targets within range are eligible for rewiring as no other edges exist. In general this is not the case.)

**Definition 4.4.** Let  $G$  be an anisotropic geometric graph with  $|V(G)| = n$ . Then we define a *rewiring* of  $G$  to be probability space over  $G_\Phi^n$ , induced by the following process: For every edge  $e \in E(G)$  uniformly at random pick a potential new target  $t'(e)$  from the set  $M_e = T_e \setminus K_e$ , where  $T_e$  is the set of all vertices that differ in their distance to  $s(e)$  less than  $\varepsilon$  from the distance of  $s(e)$  to  $t(e)$ ,

$$T_e = \{v \in V(G) \setminus s(e) \mid |d(s(e), v) - d(s(e), t(e))| < \varepsilon\}$$

and  $K_e$  the set vertices that already are connected to  $s(e)$  by another rewired edge,

$$K_e = \{v \in V(G) \mid \exists e' \in E'(G) : s(e') = s(e), t(e') = v\},$$

where  $E'(G)$  is the set of all edges that have been rewired already.

*Remark.* In the way Definition 4.4 is formulated, it is possible for  $M_e$  to be empty for an edge  $e$ . In this case no new edge is realized and the resulting, rewired network has  $|E(G)| - 1$  edges. In practice this happens less than

Let  $\tilde{C}(x)$  be the distance-dependent connectivity profile of a rewiring  $R_\varepsilon$  of an anisotropic graph  $G_{n,w}$ . Denote with  $C(x)$  the distance-dependent connection probability of the  $G_{n,w}$ . We can estimate the

$$\begin{aligned} \mathbf{E}[\tilde{C}(x)] - C(X) &= \int_{x-\varepsilon}^{x+\varepsilon} f(x') C(x') dx - C(x) \\ &= \frac{1}{2\varepsilon} \int_{x-\varepsilon}^{x+\varepsilon} C(x') - C(x) dx \\ &= \frac{1}{2\varepsilon} \left\{ \int_{x-\varepsilon}^x C(x') - C(x) dx - \int_x^{x+\varepsilon} C(x') - C(x) dx \right\} \\ &= \frac{1}{2\varepsilon} \end{aligned}$$

As a generalization of Definition 4.4, we define a partial rewiring  $R_{\varepsilon,\eta}$ , finding new targets only for a fraction  $\eta$  of all edges:

**Definition 4.5.** Let  $\varepsilon > 0$  and  $0 \leq \eta \leq 1$ . A *partial rewiring*  $R_{\varepsilon,\eta}$  of an anisotropic geometric graph  $G_{n,w}$  is then a rewiring  $R_\varepsilon$  of  $G_{n,w}$ , in which every edge is rewired with a probability of  $\eta$ , otherwise it remains. To avoid the occurrence of multiple edges,  $K_e$  is then extended to include the targets of all edges originating from  $s(e)$  that will not be rewired.

Here we choose  $\varepsilon = ??$ .

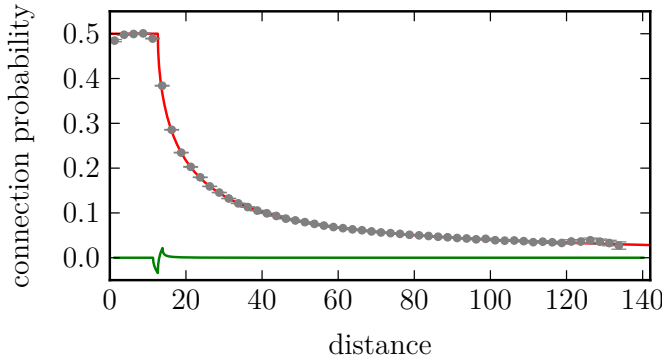


**Figure 4.11: Predicted distance-dependent connection probability profile is matched by numerical results** Averaging distance-dependent connection probabilities over the 25 sample graphs, we find the expected profile calculated in Theorem 4.3 is matched perfectly by the numerical results. (4f4dfcf1)



## 4.6 ANISOTROPY MEASURE

In the last section a method to rewire an anisotropic geometric graph, such that was introduced. From an . In this chapter we introduce.. capturing ..

The  $G_{n,\Phi}$  be a geometric graph. Then, for every is the *preferred direction* and its length is

Mardia and Jupp (2000)

**Figure 4.12:** illustrate varying levels of anisotropy

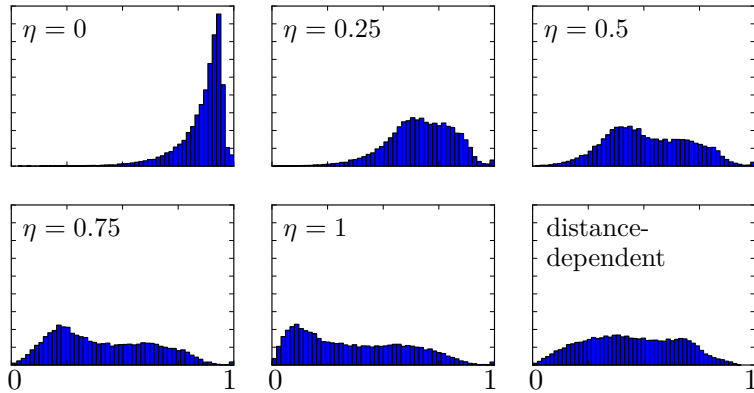


**Figure 4.13:** Rewiring significantly reduces anisotropy In data taken from the 25 sample graphs (Section 4.3), vertex isotropy degree distribution is shown for the original set of graphs ( $\eta = 0$ ) The characteristic highly anisotropic profile found in the original is already significantly reduced by partial rewiring; anisotropy degree distribution in the fully rewired graphs resemble degree distribution of equivalent purely distance-dependent networks.

... suggesting that fully rewired anisotropic networks do not . There is however one difference in out-degree as an artifact of boundary confinement (Section 5.2).

## 4.7 SUMMARY AND DISCUSSION



# 5

## STRUCTURAL ASPECTS

---

Subjecting the anisotropic network model to a critical examination of its structural features, we identify prevalent patterns of connectivity and relate theoretical and computational results to findings from experiments in the rat's visual cortex.

### 5.1 INTRODUCTION

Investigation of the brain's connectivity is an ongoing endeavour. Concurrent collaborative efforts like the Human Connectome Project [HCP], the Open Connectome Project [OCP] and the Allen Brain Atlas [ABA], intent on mapping the 'wiring' of the brain, as well as the continued development of experimental techniques and computational resources, demonstrate the great interest in advancing this field.

Research in brain connectivity spreads over the whole scale of the brain; from the mapping of fiber pathways between brain regions at the macroscopic level, to the synaptic connections of individual neurons on the microscale, researchers are trying to identify the links that enable the brain its characteristic cognitive abilities. Connections, these links are of anatomical nature. However, statistical dependencies and causal relationships between the distinct computational units in the brain are being researched with equal emphasis ([Sporns 2007](#)).

Connectivity in the context of the directionally heterogenous geometric networks introduced in Section 4.2, refers in this chapter to structural links. So far, we have only briefly mentioned that the network's nodes should be interpreted as individual neurons; to allow for a discussion of functional relationships between nodes, we have yet to provided a physical description of a neuron's function. As such, we will here explore the network's structural connectivity, modeling synaptic contacts between axon and dendrites of individual neurons.

HUMAN  
Connectome  
PROJECT  
[humanconnectome.org](http://humanconnectome.org)

Open Connectome  
Project  
[openconnectome-  
project.org](http://openconnectome-project.org)

ALLEN BRAIN ATLAS  
[brain-map.org](http://brain-map.org)

### *Synaptic Connectivity*

In the local cortical circuits the anisotropic geometric model was derived from, synaptic connectivity is a major mode of configuration. In those networks, connectivity has been determined to be neither completely random nor exclusively specific [Source]. Recurring patterns of connectivity have been identified by several reports ([Sporns and Kötter 2004](#); [Song et al. 2005](#); [Perin et al. 2011](#)).

The impact of this structural specificity discovered in local networks is shown to be significant; while the linking of network structure and network dynamics remains an active field of research, several studies were able to employ computational and theoretical models to establish such a connection. A study by Zhao et al. from 2011, for example, demonstrates how second order connectivity statistics affect a network's propensity to synchronize ([Zhao et al. 2011](#)). In the same year, Alex Roxin reported on the influence of in- and out-degree distributions on dynamics of neural network ([Roxin 2011](#)). Later, Pernice et al. were able to link structural connectivity to spike train correlations in neural networks ([Pernice et al. 2011](#)).

### *Mapping synaptic connectivity in experiments*

Experimentally, paired intracellular recordings are used to determine synaptic connectivity in cortical slices. Using two electrodes, one inserted in the cell and one outside the cell, a single intracellular recording allows for measurement of a cell's membrane potential ([Brette and Destexhe 2012](#), Chapter 3; [Weckstrom 2010](#)). Simultaneous recordings from multiple neurons are then able to infer synaptic connectivity by evoking an action potential through current injection in one neuron and observing the change of membrane potential in the other cells ([Song et al. 2005](#)).

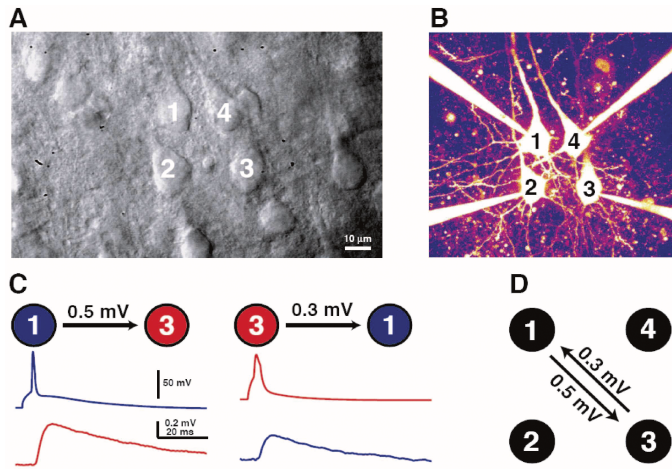


**Figure 5.1:** Song et al. use quadruple whole-cell recordings, observing simultaneously the membrane potential of four neurons. **A)** Contrast image showing four thick-tufted L5 neurons **B)** Fluorescent image of the same cells after patching on **C)** Evoking an action potential in the presynaptic neuron causes characteristic membrane potential change in the postsynaptic neuron **D)** Inferring synaptic connectivity from the EPSP waveform observed in C). Image from (Song et al. 2005).

While techniques for paired intracellular recordings are rapidly developing, their ability to capture connectivity patterns of large networks is yet very limited. To this date, the connectome of *C. Elegans* remains the outstanding exception of a connectivity configuration that has been fully mapped [Source]. Even in the state-of-the-art experiment conducted by Perin et al., using a setup capable of recording up to twelve neurons simultaneously, the authors note that an investigation of degree distribution was not carried out, due to lack of sufficient data (Perin et al. 2011).

#### *Exploiting the benefits of a geometrical model*

Working with a geometrical network model and its computational implementation, such restrictions disappear; the full information about the network, in form of its connectivity matrix, is given at point in time and can be easily queried for. Experiments that may take days to perform *in vivo*, can be completed in a matter of seconds *in silico*. As such, geometrical models lend themselves to extensive examination of their structural aspects.

*Extrapolation vs.  
reduction*

In trying to exploit these advantages, two approaches present themselves. One may construct a network model that extrapolates the known biological configuration; a full structural examination of these networks could possibly expose relevant patterns not yet observed. For this approach a sophisticated understanding of the biological configuration is critical. Neuron morphology, however, is difficult to describe and extract.

For this analysis we suggest a reductionist approach. Having motivated an abstract model reflecting a cortical network's directional heterogeneity, we distinguish emerging patterns of connectivity, specific to directionally heterogeneous networks, from results, that only indirectly stem from the network's anisotropy, in the hopes to be able to characterize the significance of directional heterogeneity in structural connectivity of cortical circuits.

*Structural aspects of the heterogeneous model*

In this chapter we subject the anisotropic network model introduced in Section 4.2 to a critical analysis of its structural aspects. General network topology, as well as specific modes and patterns of connectivity, are to be identified and laid out for comparison with findings in biological neural networks.

*employing  
anisotropy  
measure*

In an effort to map out structural features that can be directly associated with the network's directional heterogeneity, it is crucial to differentiate such findings from results that are only indirectly caused by the network's anisotropy. To this end, already in Section 4.6 we developed a measure to quantify the degree of anisotropy prevalent in a given network; throughout this chapter we will now frequently employ this measure to determine which structural aspects are originating from the network's heterogeneity, and which aspects are to be attributed solely to the network's distance dependency.

Accordingly, results from this investigation are categorized in two sections: The first section, 'Section 2', describes structural aspects that can not be directly attributed to the model's anisotropy. The second section, 'Section 3', then presents results that are truly features of network's directional heterogeneity.

## 5.2 DEGREE DISTRIBUTION

The in- and out-degree of vertex in a directed graph describes the number of incoming and outgoing connection from and to other vertices (cf. Definition 3.3). As a fundamental concept in graph and network theory, the degree distribution is integral in the categorization of networks and allows for the estimation of graph properties.

Degree distribution was shown to have strong impact on the dynamics of neuronal networks models commonly used in computational neuroscience research (Roxin 2011). Increasing in-degree variance for example could be connected to the appearance of oscillations in the network. Extracting degree distributions from biological networks however, remains a challenge as many neurons need to be tracked simultaneously to obtain enough data to confidently estimate degree distributions.

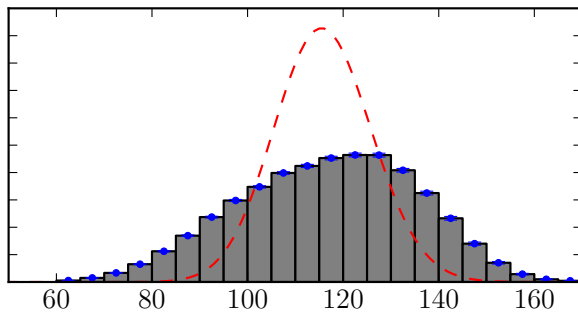


**Figure 5.2: In-degree distribution in anisotropic networks shows comparably high variance and is skewed to the left** From 250 anisotropic networks in-degree distributions were extracted and are shown in a normed histogram plot, errorbars SEM. Comparison with the binomial degree distribution (red) of a Gilbert random graph model with matching parameter set ( $N = 1000$ ,  $p = 0.116$ ) shows higher variance of in-degrees in anisotropic networks (sample variance = 344.54, variance of binomial distribution  $Np(1 - p) = 102.44$ .) Skewness to the left of the sample is  $-0.1763$ . (9326138e)

Here we analyze in- and out-degrees in the anisotropic network model. First we find that compared to the binomial in-degree distribution of a Gilbert random graph model, in-degrees of vertices in anisotropic networks display higher variance and their distribution is skewed to the left (Figure 5.2). However, this specific in-degree profile is not an intrinsic property of anisotropy, as the distribution remains stable under manipulation of the anisotropy degree and closely matches the profile of a purely distance-dependent network (Figure 5.3). This result agrees

with findings of Perin et al. (2011, Fig. S3), who were able to recreate degree distributions from their experiment with layer V thick-tufted pyramidal cells in neonatal rats from the extracted distance-dependent connection profiles alone.

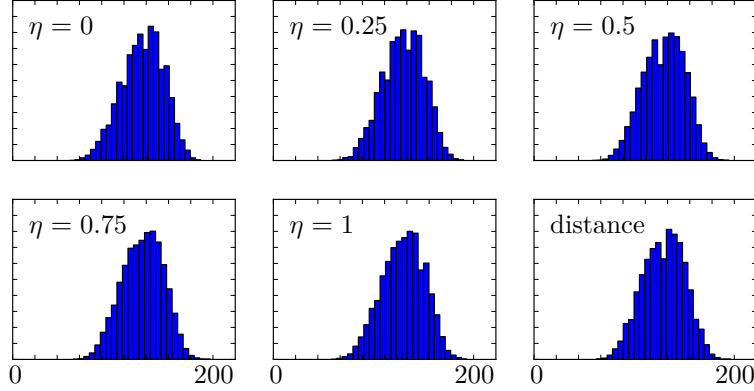


**Figure 5.3: In-degree distribution not affected by varying degrees of anisotropy** In-degree distributions from the 25 sample graphs and their rewiring stages are plotted in normed histograms and listed from rewiring factor  $\eta = 0$  (original anisotropic) to  $\eta = 1$  (completely rewired, maximal isotropy). Comparison shows that varying degrees of anisotropy do not influence the degree distribution, in fact in-degree distributions match with the degree distribution of an equivalent distance-dependent network shown bottom-right (77995b6b).

While the out-degree distribution of vertices in the anisotropic network also shows itself stable under rewiring, its distribution is drastically different from the out-degree distribution in a comparable distance-dependent network (Figure 5.4). The asymmetric, long-tailed distribution is identified as an artifact of the anisotropic network's spatial confinement; a neuron, closely located near a surface edge, might have an axon projection out of the square causing minimal out-degree or, projecting through the entire length of the surface, may have maximal out-degree. Approximating the expected number of outgoing connections for a vertex in an anisotropic network of size  $N$ , side-length  $s$  and axon width  $w$  as

$$N \frac{wl}{s^2},$$

with parameters  $N = 1000$  and  $\frac{w}{s} = 0.252$ , we obtain an upper bound for the expected out-degree,

$$N \frac{wl}{s^2} \leq N \frac{w}{s} \sqrt{2} \approx 350.$$

If  $f(l)$  is the probability density function to find axon length  $l$  for a random node  $v$  in the anisotropic network model, the out-degree distribution is then approximated by

$$\Pr[d_{\text{out}}(v) = N \frac{wl}{s^2}] = f(l), \quad (5.1)$$

see also [Figure 5.5](#).

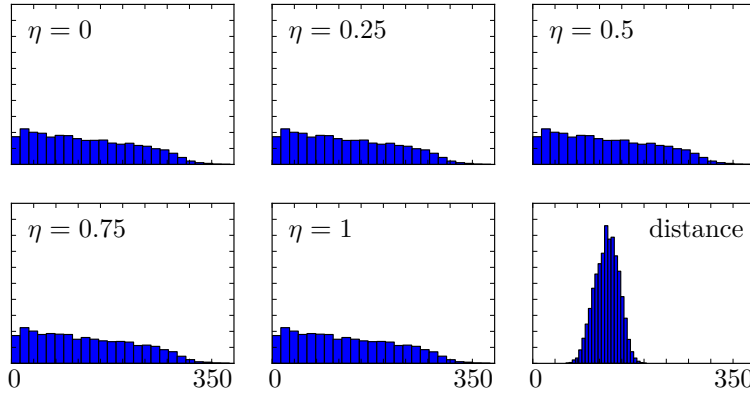


**Figure 5.4:** Out-degree distribution not affected by varying anisotropy but highly different from distance-dependent networks Out-degree distributions from the 25 sample graphs and their rewiring stages are plotted in normed histograms and listed from rewiring factor  $\eta = 0$  (original anisotropic) to  $\eta = 1$  (completely rewired, maximal isotropy). While varying degrees of anisotropy do not influence the degree distribution, the characteristic out-degree profile is drastically different from the distribution found in equivalent distance-dependent networks (77995b6b).

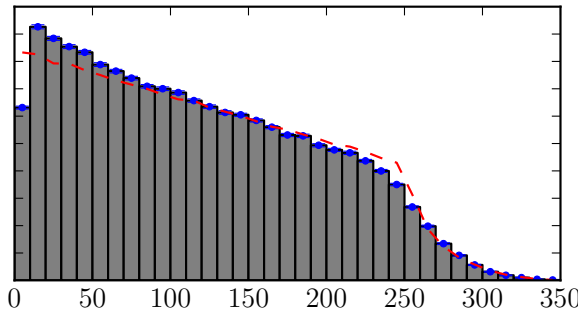


**Figure 5.5:** Characteristic out-degree distribution as an artifact of network's boundaries From 250 anisotropic networks out-degree distributions were extracted and are shown in a normed histogram plot, errorbars SEM. The characteristic distribution is identified as an artifact of the network's spatial confinement; using equation 5.1 the out-degree profile is approximated (red) by the distribution of axon lengths in the anisotropic network (019555b0).

### 5.3 SMALL WORLD PROPERTIES

Sporns papers

### 5.4 MOTIFS

## Part I

### APPENDIX



# A

## APPENDIX

---

### A.1 MATHEMATICA

```

In[1]:= f[d_] = Piecewise[{{1 / (s * (d)^(1/2)) - 1 / (s^2), 0 < d < s^2}, {0, d > s^2}}]

Out[1]= 
$$\begin{cases} -\frac{1}{s^2} + \frac{1}{\sqrt{d} s} & 0 < d < s^2 \\ 0 & \text{True} \end{cases}$$


In[2]:= g[x_] := Convolve[f[d], f[d], d, x, Assumptions -> {d ∈ Reals, x ∈ Reals}]
Simplify[g[x], {s > 0, x ∈ Reals}]

Out[3]= 
$$\begin{cases} \frac{\pi s^2 - 4 s \sqrt{x} + x}{s^4} & x > 0 \& s^2 \geq x \\ -\frac{2 s^2 + x + \frac{4 x^3}{\sqrt{-s^2+x}} - \frac{4 x}{\sqrt{-s^2+x}} - 2 s^2 \operatorname{ArcTan}\left[\frac{s}{\sqrt{-s^2+x}}\right] + i s^2 \operatorname{Log}\left[s - i \sqrt{-s^2+x}\right] - i s^2 \operatorname{Log}\left[s + i \sqrt{-s^2+x}\right]}{s^4} & s^2 < x \& 2 s^2 > x \\ 0 & \text{True} \end{cases}$$


In[4]:= h[x_] := g[x^2] * 2 * x

In[5]:= Simplify[h[x], {s > 0, x ∈ Reals, x > 0}]

Out[5]= 
$$2 x \begin{cases} \frac{\pi s^2 - 4 s x + x^2}{s^4} & s \geq x \\ -\frac{2 s^2 + x^2 + \frac{4 x^3}{\sqrt{-s^2+x^2}} - \frac{4 x^2}{\sqrt{-s^2+x^2}} - 2 s^2 \operatorname{ArcTan}\left[\frac{s}{\sqrt{-s^2+x^2}}\right] + 2 s^2 \operatorname{ArcTan}\left[\frac{\sqrt{-s^2+x^2}}{s}\right]}{s^4} & s < x \& \sqrt{2} s > x \\ 0 & \text{True} \end{cases}$$


In[6]:= (*For s == 1, h becomes*)

In[7]:= Simplify[h[x], {s == 1, x ∈ Reals, x > 0}]

Out[7]= 
$$2 x \begin{cases} \pi + (-4 + x) x & x \leq 1 \\ -2 - x^2 + 4 \sqrt{-1 + x^2} - 2 \operatorname{ArcCot}\left[\frac{1}{\sqrt{-1+x^2}}\right] + 2 \operatorname{ArcTan}\left[\frac{1}{\sqrt{-1+x^2}}\right] & 1 < x < \sqrt{2} \\ 0 & \text{True} \end{cases}$$


In[8]:= (*Expected Value*)
s := 1.
Integrate[x * h[x], {x, 0, Sqrt[2]}]

Out[9]= 0.521405

```

**Mathematica A.1:** Computation of probability density function for distance between two random points in square of side length  $s$  as supplement to proof of Theorem 3.12. Note that form of final result Out[7] differs from solution given in 3.12. While proof of equivalence could not be achieved analytically, expressions given are numerically equivalent, see Mathematica A.2.

```

In[1]:= f[d_] = Piecewise[{{1 / (s * (d)^(1/2)) - 1 / (s^2), 0 < d < s^2}, {0, d > s^2}}]

Out[1]= 
$$\begin{cases} -\frac{1}{s^2} + \frac{1}{\sqrt{d}} & 0 < d < s^2 \\ 0 & \text{True} \end{cases}$$


In[2]:= g[x_] := Convolve[f[d], f[d], d, x, Assumptions -> {d ∈ Reals, x ∈ Reals}]
Simplify[g[x], {s > 0, x ∈ Reals}]

Out[3]= 
$$\begin{cases} \frac{\pi s^2 - 4 s \sqrt{x} + x}{s^4} & x > 0 \& s^2 \geq x \\ -\frac{2 s^2 + x + \frac{4 s^3}{\sqrt{-s^2+x}} - \frac{4 s x}{\sqrt{-s^2+x}} - 2 s^2 \operatorname{ArcTan}\left[\frac{s}{\sqrt{-s^2+x}}\right] + i s^2 \operatorname{Log}[s - i \sqrt{-s^2+x}] - i s^2 \operatorname{Log}[s + i \sqrt{-s^2+x}]}{s^4} & s^2 < x \& 2 s^2 > x \\ 0 & \text{True} \end{cases}$$


In[4]:= h[x_] := g[x^2] * 2 * x

In[5]:= Simplify[h[x], {s > 0, x ∈ Reals, x > 0}]

Out[5]= 
$$2 x \begin{cases} \frac{\pi s^2 - 4 s x + x^2}{s^4} & s \geq x \\ -\frac{2 s^2 + x^2 + \frac{4 s^3}{\sqrt{-s^2+x^2}} - \frac{4 s x^2}{\sqrt{-s^2+x^2}} - 2 s^2 \operatorname{ArcTan}\left[\frac{s}{\sqrt{-s^2+x^2}}\right] + 2 s^2 \operatorname{ArcTan}\left[\frac{\sqrt{-s^2+x^2}}{s}\right]}{s^4} & s < x \& \sqrt{2} < x \\ 0 & \text{True} \end{cases}$$


In[6]:= (*For s = 1, h becomes*)

In[7]:= Simplify[h[x], {s = 1, x ∈ Reals, x > 0}]

Out[7]= 
$$2 x \begin{cases} \pi + (-4 + x) x & x \leq 1 \\ -2 - x^2 + 4 \sqrt{-1 + x^2} - 2 \operatorname{ArcCot}\left[\frac{1}{\sqrt{-1+x^2}}\right] + 2 \operatorname{ArcTan}\left[\frac{1}{\sqrt{-1+x^2}}\right] & 1 < x < \sqrt{2} \\ 0 & \text{True} \end{cases}$$


In[8]:= (*Expected Value*)
s := 1.
Integrate[x * h[x], {x, 0, Sqrt[2]}]

Out[9]= 0.521405

```

**Mathematica A.2:** Computation of probability density function for distance between two random points in square of side length  $s$  as supplement to proof of Theorem 3.12. Note that form of final result Out[7] differs from solut

## A.2 SUPPLEMENTARY FIGURES

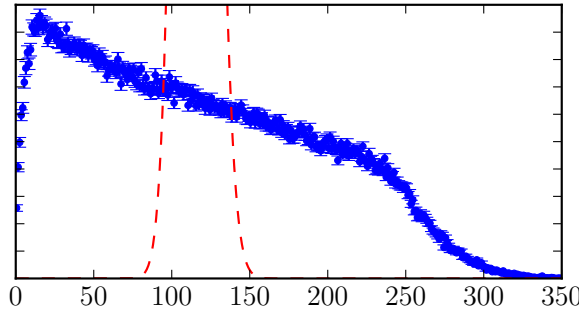


Figure A.1: (c7ee86d7)

## BIBLIOGRAPHY

---

- Bang-Jensen, Jørgen and Gregory Z. Gutin (2008). *Digraphs: Theory, Algorithms and Applications*. 2nd ed. London: Springer. DOI: 10.1007/978-1-84800-998-1.
- Bollobás, Béla (2001). *Random graphs*. 2nd ed. Cambridge University Press.
- Braitenberg, Valentino and A Schüz (1998). *Cortex: Statistics and Geometry of Neuronal Connectivity*. 2nd ed. Berlin; New York: Springer.
- Brette, Romain and Alain Destexhe (2012). *Handbook of neural activity measurement*. Cambridge: Cambridge University Press.
- Debanne, Dominique (2004). Information processing in the axon. *Nature Reviews Neuroscience* 5.4, pp. 304–316.
- Diestel, Reinhard (2000). *Graph Theory*. 2nd ed. Vol. 173. Graduate Texts in Mathematics. Springer-Verlag, New York.
- Erdős, P. and A. Rényi (1959). On random graphs, I. *Publicationes Mathematicae (Debrecen)* 6, pp. 290–297.
- Feldman, M.L. (1984). Morphology of the neocortical pyramidal neuron. *Cerebral cortex, Vol 1, Cellular components of the cerebral cortex*. Ed. by Alan Peters and Edward G Jones. New York: Plenum Press, pp. 123–200.
- Gilbert, E. N. (1959). Random Graphs. *The Annals of Mathematical Statistics* 30.4, pp. 1141–1144. DOI: 10.1214/aoms/1177706098.
- Gilbert, E.N. (1961). Random Plane Networks. *Journal of the Society for Industrial and Applied Mathematics* 9.4, pp. 533–543. DOI: 10.1137/0109045.
- Ishizuka, Norio, Janet Weber, and David G Amaral (1990). Organization of intrahippocampal projections originating from CA3 pyramidal cells in the rat. *Journal of Comparative Neurology* 295.4, pp. 580–623.
- Janson, S., T. Łuczak, and A. Rucinski (2000). *Random Graphs*. Wiley Series in Discrete Mathematics and Optimization. Wiley.
- Łuczak, Tomasz (1990). On the equivalence of two basic models of random graph. *Proceedings of Random graphs*. Vol. 87, pp. 151–157.
- Mardia, Kanti V. and Peter E. Jupp (2000). *Directional Statistics*. 2nd ed. John Wiley & Sons Ltd.

- Moltchanov, D. (2012). Distance distributions in random networks. *Ad Hoc Networks* 10.6, pp. 1146–1166. DOI: 10.1016/j.adhoc.2012.02.005.
- Penrose, Mathew (2003). *Random Geometric Graphs (Oxford Studies in Probability)*. Oxford University Press, USA.
- Perin, Rodrigo, Thomas K. Berger, and Henry Markram (2011). A synaptic organizing principle for cortical neuronal groups. *Proceedings of the National Academy of Sciences* 108.13, pp. 5419–5424. DOI: 10.1073/pnas.1016051108.
- Pernice, Volker, Benjamin Staude, Stefano Cardanobile, and Stefan Rotter (2011). How Structure Determines Correlations in Neuronal Networks. *PLoS Comput Biol* 7.5, e1002059. DOI: 10.1371/journal.pcbi.1002059.
- Petersen, Carl C. H., Amiram Grinvald, and Bert Sakmann (2003). Spatiotemporal Dynamics of Sensory Responses in Layer 2/3 of Rat Barrel Cortex Measured In Vivo by Voltage-Sensitive Dye Imaging Combined with Whole-Cell Voltage Recordings and Neuron Reconstructions. *The Journal of Neuroscience* 23.4, pp. 1298–1309.
- Philip, J. (2007). The probability distribution of the distance between two random points in a box. TRITA MAT 07 MA 10.
- Ramaswamy, Srikanth, Sean L Hill, James G King, Felix Schürmann, Yun Wang, and Henry Markram (2012). Intrinsic morphological diversity of thick-tufted layer 5 pyramidal neurons ensures robust and invariant properties of in silico synaptic connections. *The Journal of physiology* 590.4, pp. 737–752.
- Ramon, Y and S Cajal (1911). Histologie du systeme nerveux de l'homme et des vertebres. *Maloine, Paris* 2, pp. 153–173.
- Romand, Sandrine, Yun Wang, Maria Toledo-Rodriguez, and Henry Markram (2011). Morphological development of thick-tufted layer V pyramidal cells in the rat somatosensory cortex. *Frontiers in Neuroanatomy* 5.5. DOI: 10.3389/fnana.2011.00005.
- Ropireddy, Deepak, Ruggero Scorcioni, Bonnie Lasher, Gyorgy Buzsáki, and GiorgioA. Ascoli (2011). Axonal morphometry of hippocampal pyramidal neurons semi-automatically reconstructed after in vivo labeling in different CA3 locations. *Brain Structure and Function* 216.1, pp. 1–15. DOI: 10.1007/s00429-010-0291-8.
- Roxin, Alex (2011). The Role of Degree Distribution in Shaping the Dynamics in Networks of Sparsely Connected Spiking Neurons. *Frontiers in Computational Neuroscience* 5. DOI: 10.3389/fncom.2011.00008.
- Simpson, Thomas (1755). A letter to the Right Honourable George, Earl of Macclesfield, President of the RoyalSociety, on the advan-

- tage of taking the mean of a number of observations in practical astronomy. *Phil. Trans. R. Soc. Lond* 49, pp. 82–93.
- Song, Sen, Per Jesper Sjöström, Markus Reigl, Sacha Nelson, and Dmitri B Chklovskii (2005). Highly Nonrandom Features of Synaptic Connectivity in Local Cortical Circuits. *PLoS Biol* 3.3, pp. 507–519. DOI: 10.1371/journal.pbio.0030068.
- Sporns, Olaf (2007). Brain connectivity. *Scholarpedia* 2.10, p. 4695. DOI: 10.4249/scholarpedia.4695.
- Sporns, Olaf and Rolf Kötter (2004). Motifs in Brain Networks. *PLoS Biol* 2.11, e369. DOI: 10.1371/journal.pbio.0020369.
- Stepanyants, Armen and Dmitri B. Chklovskii (2005). Neurogeometry and potential synaptic connectivity. *Trends in Neurosciences* 28.7, pp. 387 –394. DOI: 10.1016/j.tins.2005.05.006.
- Stepanyants, Armen, Patrick R. Hof, and Dmitri B. Chklovskii (2002). Geometry and Structural Plasticity of Synaptic Connectivity. *Neuron* 34.2, pp. 275 –288. DOI: 10.1016/S0896-6273(02)00652-9.
- Weckstrom, Matti (2010). Intracellular recording. *Scholarpedia* 5.8, p. 2224. DOI: 10.4249/scholarpedia.2224.
- Zhao, Liqiong, Bryce Beverlin, Theoden Netoff, and Duane Q. Nykamp (2011). Synchronization from Second Order Network Connectivity Statistics. *Frontiers in Computational Neuroscience* 5. DOI: 10.3389/fncom.2011.00028.



## INDEX

---

anisotropic geometric  
graph, 24  
random graph model, 24  
apical dendrite, 20  
  
basal dendrite, 20  
binomial random graph, 11  
  
directed graph, 5  
distance-dependent  
connection probability, 12  
random graph model, 12  
  
geometric graph, 12  
Gilbert random graph model, 10  
  
in-degree, 7  
  
loop graph, 5  
  
multigraph, 5  
  
neuro geometry, 18  
  
out-degree, 7  
  
potential synapse, 18  
preferred direction, 33  
pseudograph, 5  
  
random graph, 10  
  
simple graph, 5  
  
weighted graph, 6

<b>Symbol</b>	<b>Description</b>
$L$	Length
$Ma$	Mach number
$p$	Pressure